frontiers in Earth Science

ORIGINAL RESEARCH
published: 16 April 2021
doi: 10.3389/feart.2021.633713

Applicability and Variability of Chemical Weathering Indicators and Their Monsoon-Controlled Mechanisms in the Bay of Bengal

Jingrui Li[1,2], Shengfa Liu[1,2], Xuefa Shi[1,2], Hui Zhang[1,2], Peng Cao[1,2], Xiaoyan Li[1,2], Hui-Juan Pan[3,4], Somkiat Khokiattiwong[5] and Narumol Kornkanitnan[5]*

[1] Key Laboratory of Marine Geology and Metallogeny, First Institute of Oceanography, Ministry of Natural Resources, Qingdao, China, [2] Laboratory for Marine Geology, Qingdao National Laboratory for Marine Science and Technology, Qingdao, China, [3] Institute of Earth Sciences, College of Ocean Science and Resource, National Taiwan Ocean University, Keelung, Taiwan, [4] Center of Excellence for Ocean Engineering, College of Engineering, National Taiwan Ocean University, Keelung, Taiwan, [5] Department of Marine and Coastal Resources, Marine and Coastal Resources Research and Development Institute, Bangkok, Thailand

OPEN ACCESS

Edited by:
Gary E. Stinchcomb,
Murray State University, United States

Reviewed by:
William Ellis Lukens,
James Madison University, United States
Anil Shukla,
Physical Research Laboratory, India
Yongbo Wang,
Capital Normal University, China

***Correspondence:**
Xuefa Shi
xfshi@fio.org.cn

Specialty section:
This article was submitted to Quaternary Science, Geomorphology and Paleoenvironment, a section of the journal Frontiers in Earth Science

Received: 26 November 2020
Accepted: 29 March 2021
Published: 16 April 2021

Citation:
Li J, Liu S, Shi X, Zhang H, Cao P, Li X, Pan H-J, Khokiattiwong S and Kornkanitnan N (2021) Applicability and Variability of Chemical Weathering Indicators and Their Monsoon-Controlled Mechanisms in the Bay of Bengal. Front. Earth Sci. 9:633713. doi: 10.3389/feart.2021.633713

To help understanding the potential relationship between chemical weathering and Indian summer monsoon (ISM) since the last glacial period a gravity core (BoB-56) was retrieved from the central Bay of Bengal (BoB). The data of chemical weathering indexes (CIA, WIP, and α^{Al}Na) used in this study showed general synchronicity with the regional monsoon precipitation and temperature record on precessional scale, indicating existence of control from the ISM on weathering. Corresponding to alteration of warm/cold period during the last deglaciation, obvious simultaneously alteration of higher/lower values of the chemical weathering and terrestrial input proxies' record support our hypothesis that the ISM driving chemical weathering on the millennial scale. However, a contradiction occurred during the Holocene period, when the ISM precipitation and temperature rose to a higher level, while the alternative indexes unanimously reflected a weaker chemical weathering conditions. In this study, we discussed the applicability of chemical weathering indexes in the BoB during the Holocene period. Besides the possible weakened monsoon during 6–3 ka, recorded by the stalagmite $\delta^{18}O$ and Sea Surface Temperature (SST) reconstruction results in the northeastern Indian Ocean, other factors were responsible for this phenomenon, including the grain size effect and distinction between the mountain high land and floodplain low land. The chemical weathering records, during the last glaciation, indicated the presence of control from the ISM on weathering at precessional and millennial scales. While, during the Holocene, they failed to reflect the actual chemical weathering dynamics of the source area. Indeed, a mixture of physical erosion and chemical weathering seems to be representative of the chemical weathering dynamics in the area. Our findings emphasized on the tight connections between the chemical weathering evolution and global-regional climate conditions around the BoB, implying possible ISM-controlled mechanisms during different time scales.

Keywords: geochemistry, chemical weathering, Indian summer monsoon, precipitation, Bay of Bengal

INTRODUCTION

Chemical weathering is one of the most important processes of the earth's elemental cycle, especially for the carbon cycle, and is closely related to tectonic, climatic, and environmental factors (Walker et al., 1981; Berner, 1992; Gaillardet et al., 1999; Yang et al., 2004a; Eiriksdottir et al., 2011; Miriyala et al., 2017; He et al., 2020; Liu et al., 2020). During the journey from "source" to "sink," particles carry source chemical weathering signals to the sink area, which are interfered and modified by path signals, and form strata, containing chemical weathering signals. Therefore, deciphering the chemical weathering intensity records in stratigraphic signals can provide us with information on the environmental evolution in source regions at different time scales, helping to understand the different control mechanisms of chemical weathering. From the transportation characteristics of environmental signals in the process of "source-sink," the stronger the signal in the source area, the shorter the transformation time, and the more stable and continuous the strata are, the more conducive to the decoding of environmental signals (Romans et al., 2016). In addition, the obvious tectonic and climatic signals in the source area are likely to be masked, modified, or damaged by other signals during transportation (Jerolmack and Paola, 2010; Romans et al., 2016), such as fluvial-floodplain processes, which are not affected by the original upstream signals. Located back against "the roof of the world," the Tibetan Plateau, the Bay of Bengal (BoB) is considered as the supergiant source of sediment in the Asian continent margin, with a mixture of world-class high mountain terrain and low relief develop in the foreland like flood plain, combined with the developed river systems. In addition to the world-class delta, the BoB has developed a largest submarine fan in the world. Typical Indian monsoon climate affects the whole BoB and surrounding areas. The drilling results show that except for the early Eocene and late Miocene, the remaining strata are relatively continuous (Curray and Moore, 1971), providing us with a good target for deciphering regional chemical weathering evolution and its control mechanism, and recorded in the sediment strata.

Tectonics, climate, and sea level fluctuations have significant control on generating, transportation, and preservation of the chemical weathering signals. Overall, the major tectonics around the BoB remained stable during the last glaciation scale. The sediment in the BoB are mainly transported from the Ganges-Brahmaputra River (hereinafter referred to as "G-B" River), so the influence from tectonic characteristics is mainly reflected in the difference between the composition of the high mountainous terrain in the upper reaches and the low plain terrain in the middle and lower reaches (Joussain et al., 2016; Yu et al., 2020). The sea level mainly controls the relative input between the delta-shelf and the deep sea on a glacial-interglacial scale (Li et al., 2019). Regardless of long or short time scales, climate change seems to be the closest factor, controlling the chemical weathering, with two basic parameters, i.e., the precipitation and temperature (Liu et al., 2020). The "competition" among these factors has been maintained throughout the late Quaternary in the area and preserved in the sediments, transported by rivers into the ocean. In the northeast Indian Ocean, the Indian monsoon climate change, recorded by ocean indexes since the last glaciation, mainly embodied in glacial-interglacial, precessional and millennial scales variations, subjected to the global ice condition, the latitude distribution distinction of solar radiation, caused by the earth parameters, and the millennial climate events in the high latitudes of the northern hemisphere, respectively (Duplessy, 1982; Prell and Kutzbach, 1987; Schulz et al., 1998; Clemens and Prell, 2003; Gupta et al., 2005; Caley et al., 2011; Bolton et al., 2013; Cao et al., 2015; Mohtadi et al., 2016; Raza et al., 2017). These periodic changes are recorded in the marine sedimentary strata and have been subjected to study in several research (Clemens and Prell, 2003; Cao et al., 2015; Li et al., 2018, 2019, 2020; Sebastian et al., 2019; Liu et al., 2020; Yu et al., 2020). If the chemical weathering evolution in the BoB is mainly controlled by the Indian monsoon climate, one or more of the above periodic changes should have occurred in its temporal variation trend. Indian monsoon rainfall is mainly concentrated in the summer monsoon period, accounting for more than 90% of the annual precipitation (Rodolfo, 1969; Singh et al., 2007). Therefore, summer monsoon rainfall can be regarded as a typical alternative index of Indian monsoon intensity and its time-evolution characteristics and control mechanism are stablished in a large number of studies (Prell and Kutzbach, 1987; Schulz et al., 1998; Kudrass et al., 2001; Fleitmann et al., 2003, 2007; Rashid et al., 2007; Bolton et al., 2013), which are used as references for our comparative analysis.

Element molar contents based proxies, e.g., Chemical Index of Alteration (CIA; Nesbitt and Young, 1982), Weathering Index of Parker (1970), and α^{Al}E (Garzanti et al., 2013), have been successfully applied in different sedimentary environments to estimate the chemical weathering intensity (Liu et al., 2013, 2020; Li et al., 2017; Xu et al., 2018). It should be noted that the variation of geochemical element content is controlled not only by the changes in chemical weathering intensity, but also by the mixing process of sediment particles from different sources or various components. Therefore, while applying the above parameters, the influence of provenance factors needs to be taken into account. In this study, these three commonly used chemical weathering index parameters, i.e., CIA, WIP, and α^{Al}E are analyzed to evaluate the chemical weathering dynamics around the BoB and its response to the Indian monsoon climate, since the last glaciation. Meanwhile, the application of geochemical parameters, represented by the CIA are discussed to estimate the chemical weathering dynamics in different stages. The findings from this study can help to build a "climate-weathering-sedimentation" connection in the BoB.

MATERIALS AND METHODS

Materials

Core BoB-56 (location: 16.56°N, 88.55°E; length: 3.41 m; water depth: 2,615 m; **Figure 1**) was collected from the central BoB in 2012, during China-Thailand BoB joint scientific cruise. The general procedures of the Key Laboratory of Marine Geology and Metallogeny, Ministry of Natural Resources, China, was followed as a pre-treatment procedure, including a detailed core

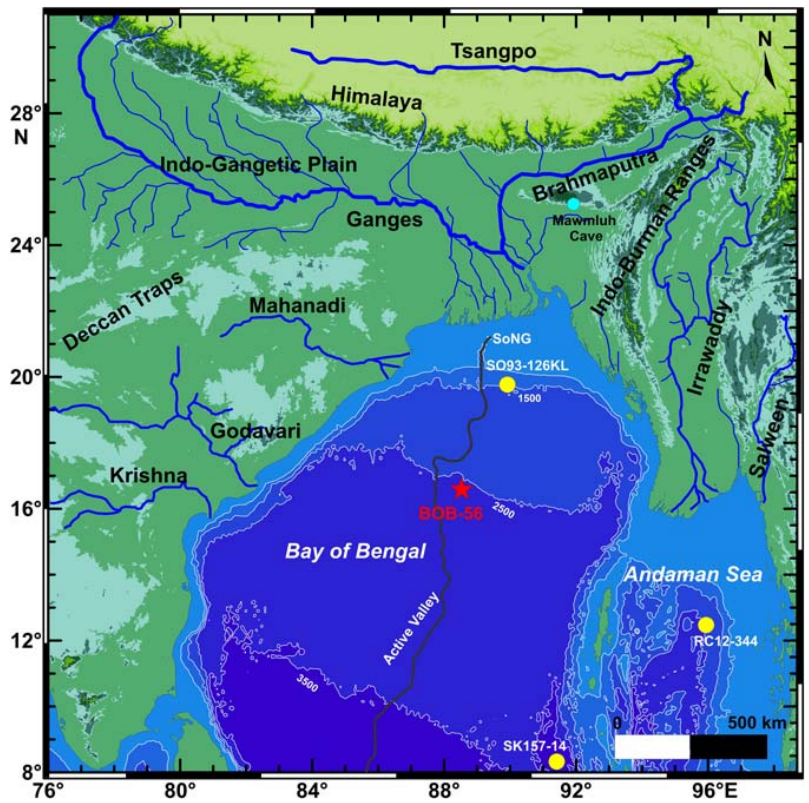

FIGURE 1 | Location of the BoB. The core BoB-56 and referenced cores are marked by red stars and yellow circles, respectively. The cyan color circle in the land show location of the Mawmluh Cave. SoNG: Swatch of No Ground, the largest submarine canyon in the BoB.

description and sub-samples division. Briefly, sediments of core BoB-56 were composed of relatively homogeneous gray clay silt except the upper 30 cm which showed the yellow brown color mainly due to the relative higher sand fraction. Grain size and geochemical analyses were carried out on the 2 cm intervals. AMS ^{14}C age model was constructed based on mixed planktonic foraminifera species (**Figure 2**; Li et al., 2018). Downcore ages were calculated by linear interpolation between dated sediment layers and the bottom age is 40.0 ka BP. Correspondingly, the sedimentation rates during the Holocene period (∼3.1 cm/kyr) were lower than those during the last glacial and deglacial periods (∼10.9 cm/kyr). The chronology, grain size, and part of element geochemistry (Ti, Ca, Rb, Sr, and Ba) compositions have been reported in our previous work (Li et al., 2018, 2019). In particular, sediment provenance of the core BoB-56 has been identified using Sr and Nd isotope compositions (Li et al., 2018), which confirmed that most of the sediments are from the Himalayas. This could decrease the difficulty of interpretation of weathering signal due to the complex sediment sources, and improve the reliability of the indexes.

Geochemical Analyses

Each frozen and dried sample with a weight of 0.05 g was placed in a polytetrafluoroethylene digestion tank, dissolved twice in HF-HNO_3 (1:1), and dried at 190°C for 48 h. Subsequently, by reacting with 1 mL of HNO_3, the residual HF was removed and the samples were digested with a mixture of 3 mL of 50% HNO_3 and 1 mL of Rh (500 ppb) for 24 h in an oven at 150°C. Then, 50 g of the mixture was prepared for element concentration analyses using Inductively Coupled Plasma Optical Emission Spectrometry. 10% of these samples were analyzed repeatedly, to determine the measurement error. The GSD-9 reference standard was also measured to confirm the accuracy and an approximately 5% measurement error was determined.

Chemical Weathering Indexes Calculation

Three element molar contents based proxies, CIA (Nesbitt and Young, 1982), Weathering Index of Parker (WIP; Parker, 1970) and α^{Al}E (Garzanti et al., 2013) were applied in this study to evaluate the chemical weathering conditions, and the calculation formulas are as follows:

$$\mathrm{CIA} = \mathrm{Al_2O_3}/(\mathrm{Al_2O_3} + \mathrm{CaO^*} + \mathrm{Na_2O} + \mathrm{K_2O}) \times 100 \quad (1)$$

$$\mathrm{WIP} = (2\mathrm{Na_2O}/0.35 + \mathrm{MgO}/0.9 + 2\mathrm{K_2O}/0.25 + \mathrm{CaO^*}/0.7) \times 100 \quad (2)$$

$$\alpha^{\mathrm{Al}}\mathrm{E} = (\mathrm{Al/E})_{\mathrm{sediment}} / (\mathrm{Al/E})_{\mathrm{UCC}} \quad (3)$$

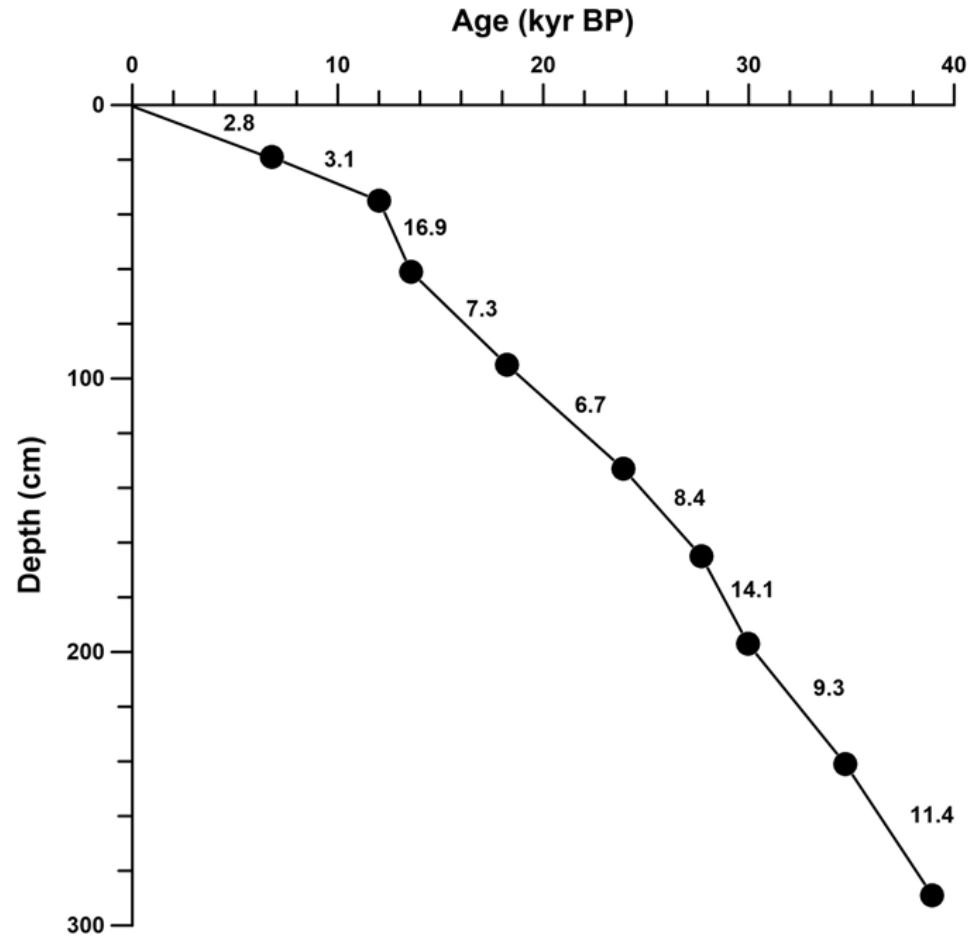

FIGURE 2 | Depth versus calibrated AMS^{14}C age and linear sedimentation rate (LSR) plots of core BoB-56 (Li et al., 2018). The LSR is listed for each interval in cm/kyr.

Where, CaO* refers to CaO contents in the silicate. In this study, the method from Mclennan et al. (1993) was adopted to approximately correct the CaO* content for the presence of Ca in carbonates (calcite and dolomite) and phosphates (apatite). CaO was corrected for phosphate using P_2O_5. If the remaining number of moles is less than that of Na_2O, this CaO value is adopted. Otherwise, CaO* is assumed to be equivalent to Na_2O. In this method, minimum CIA values could be yielded since the Ca lost more rapidly than Na during weathering. UCC refers to the Upper Continental Crust (Taylor and Mclennan, 1985). In this study, E = Na.

Principal Component Analysis

To better extract the inner regularities and further constrain the controlling mechanisms of the chemical weathering indexes, the principal component analysis (PCA) is performed for these chemical weathering dataset (CIA, WIP, and α^{Al}Na), using the IBM SPSS Statistics 19.0 software. Generally, three conditions must be satisfied, including sufficient samples (at least five times the number of variables), a strong correlation between the original data (the Bartlett test of sphericity yields a value under 0.05 or the KMO measure of sampling adequacy is above 0.5), and significant common factors obtained (factor rotation if necessary). In this study, 441 data points are used and the Bartlett test of sphericity/the KMO measure of sampling adequacy yields values 0 and 0.64. Then, controlling factors with eigen value above 1 were extracted and the rotating component matrix was gotten by Maximum-variance Algorithm. Comparing with the climatic proxies, detailed variations and controlling mechanisms of chemical weathering intensity on different timescales were discussed.

RESULTS

Geochemical Composition Variations

The geochemical compositions and downcore variations of core BoB-56 sediments are presented in **Figure 3**. Al_2O_3, K_2O, and TiO_2 appear to vary synchronously, while the CaO contents tend to be a mirror trend. Na_2O shows a roughly similar average contents between the Last Glaciation and the Holocene periods, but a decreased trend since the Holocene period. Overall, higher

contents of CaO are observed during the Holocene period and lower contents during the last glaciation. Meanwhile, opposite pattern is identified for other oxides. Alternation of high and low values could be seen during the last deglaciation. The major oxides contents, i.e., Al_2O_3, K_2O, TiO_2, CaO, and Na_2O range between 11.61 and 16.87%, 2.22 and 3.76%, 0.54 and 0.84%, 1.64 and 4 13.84%, and 2.13 and 3.06%, respectively, with average contents of 15.03, 3.00, 0.72, 6.39, and 2.60%, respectively. Similar to the geochemistry variations, sand fractions of core BoB-56 sediment show significantly higher volume contents during the Holocene period (averaged 7.08%), compared to the last glaciation (averaged 0.62%).

Chemical Weathering Intensity Estimation

Three chemical weathering indexes, including CIA, WIP, and α^{Al}Na used in this study are shown in **Figure 4**. All these indexes

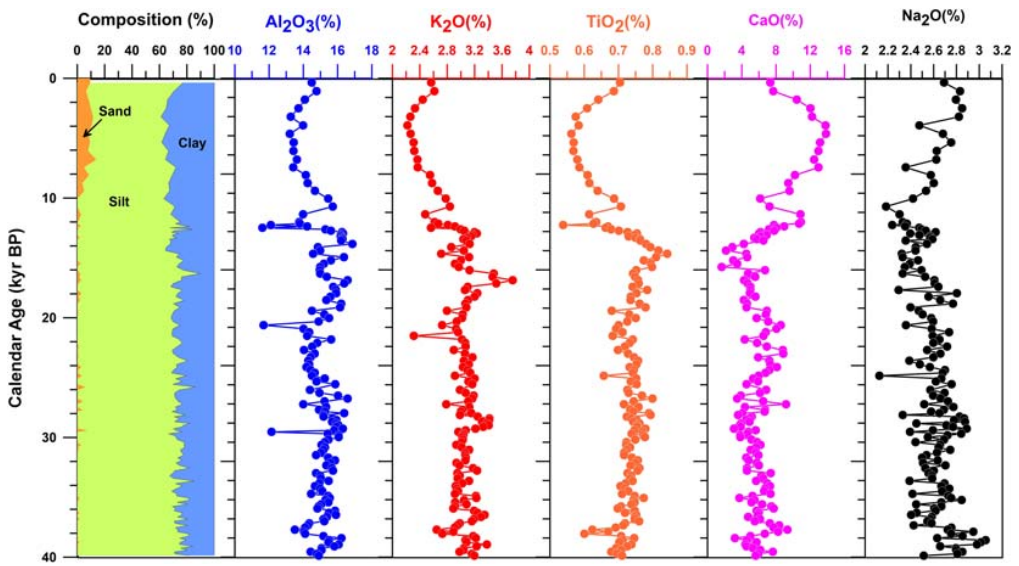

FIGURE 3 | Downcore variations of grain size (Li et al., 2018) and elemental composition in the core BoB-56.

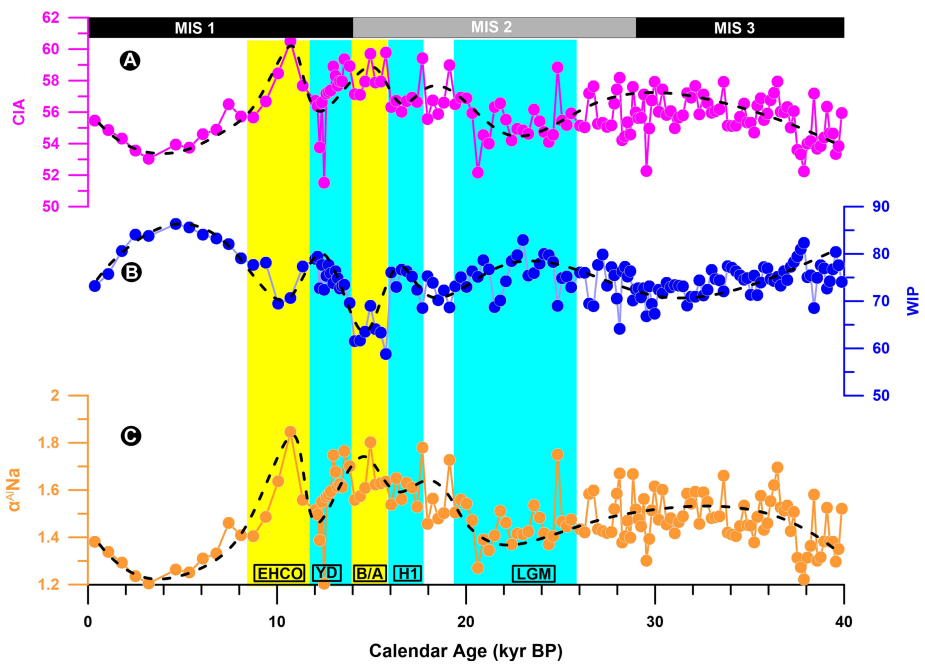

FIGURE 4 | Downcore variations of the chemical weathering indexes. **(A)** CIA; **(B)** WIP; and **(C)** α^{Al}Na.

TABLE 1 | Factor analysis of CIA, WIP, αAlNa, and extraction of three factors with eigen values > 1.

	F1	F2	F3
Eigen value	2.44	0.52	0.04
% variation	81.41	17.22	1.37
CIA	0.94	–0.31	0.14
WIP	-0.28	0.96	–0.06
α^{Al}Na	0.96	–0.26	–0.11

indicate a relatively weak chemical weathering condition on the whole. Within the current chronology frame, two precessional cycles (40–20 ka and 20 ka to present) can be identified through the whole cores. Two obvious low values are associated with the Last Glacial Maximum (LGM) and the Holocene period. However, the latter cycle (20 ka to present) shows a distinct peak with higher frequency oscillation, indicating that the elemental data might more closely follow higher-frequency event [e.g., Heinrich 1 (H1), Bølling/Allerød (B/A), Younger Dryas (YD), and Early Holocene Climate Optimum]. Actually, it reminds us of a millennial scale variation for the chemical weathering intensity. Briefly, the results exhibit that the chemical weathering proxies vary in two different cycles, precessional, and millennial cycles.

Principal Component Analysis of Chemical Weathering Indexes

The PCA results show that three components with eigen value above 1 could be extracted and 81% of common variance could be explained by the first component (F1; **Table 1**), clearly suggesting that the variations of chemical weathering proxies are mainly controlled by the same driving force. Considering the typical monsoon climate around the BoB and close relationship between climate and weathering (Romans et al., 2016; Liu et al., 2020), simultaneously compared downcore variations of F1 with the Indian summer monsoon (ISM) records in and around the BoB (**Figures 5**, **7**; Kudrass et al., 2001; Rashid et al., 2007; Berkelhammer et al., 2012; Raza et al., 2017), we could initially conclude that F1 represents control from the ISM, due to the covariant relationship between chemical weathering indexes (CIA and α^{Al}Na) and F1 (**Table 1** and **Figures 4**, **5**).

However, 20% of the elemental weathering signal is lost to other processes, mainly the F2 which could interpret 19% of the variations, and the main proxy controlled by F2 is the WIP (**Table 1** and **Figure 6A**). Comparing the calculation formulas of three chemical weathering proxies used in this study, the main difference between the WIP and the others is the MgO which is not contained in the CIA and α^{Al}Na. We plot F2 and these three proxies and MgO, CaO, Al_2O_3, K_2O, and Na_2O in the binary scatter diagram (**Figure 6**). It shows significant correlation between F2 and the WIP (R^2 = 0.90), but distinct expression between F2 and oxides during the last glaciation and the Holocene period. Positive correlation occurred between F2 and MgO, CaO during the last glaciation (R^2 = 0.39, 0.55, respectively), and significant positive correlation between F2 and CaO (R^2 = 0.97), negative correlation between F2 and MgO, Al_2O_3, and K_2O (R^2 = 0.89, 0.76, and 0.73, respectively) during the Holocene period could be seen. Na_2O shows nothing to do

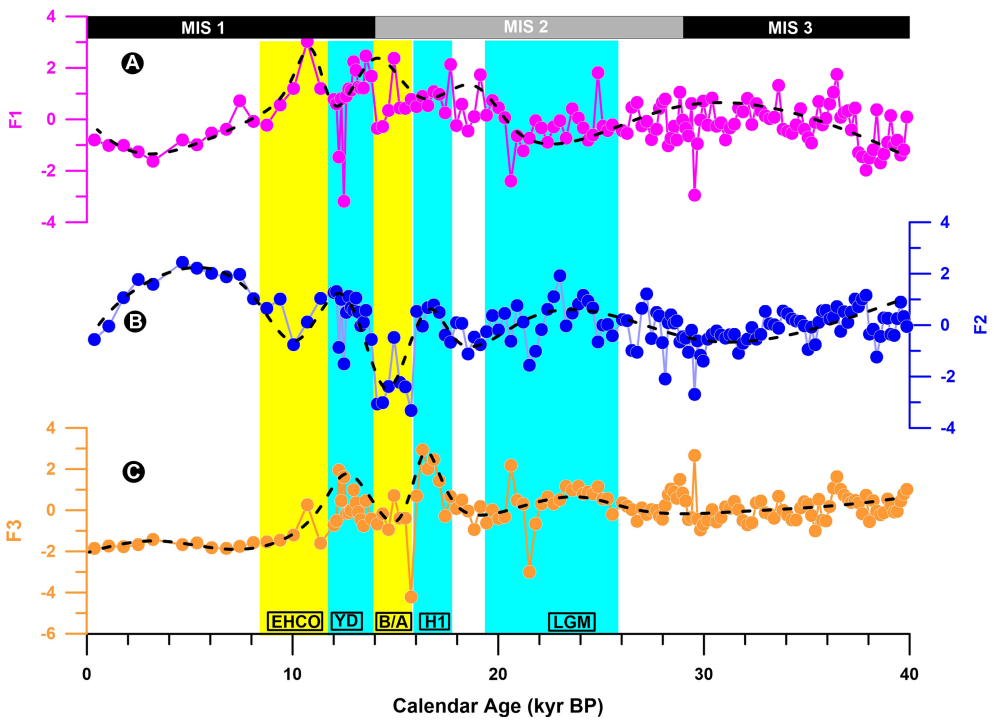

FIGURE 5 | Downcore variations of PCA components scores. **(A)** Curves of F1 scores; **(B)** curves of F2 scores; **(C)** curves of F3 scores.

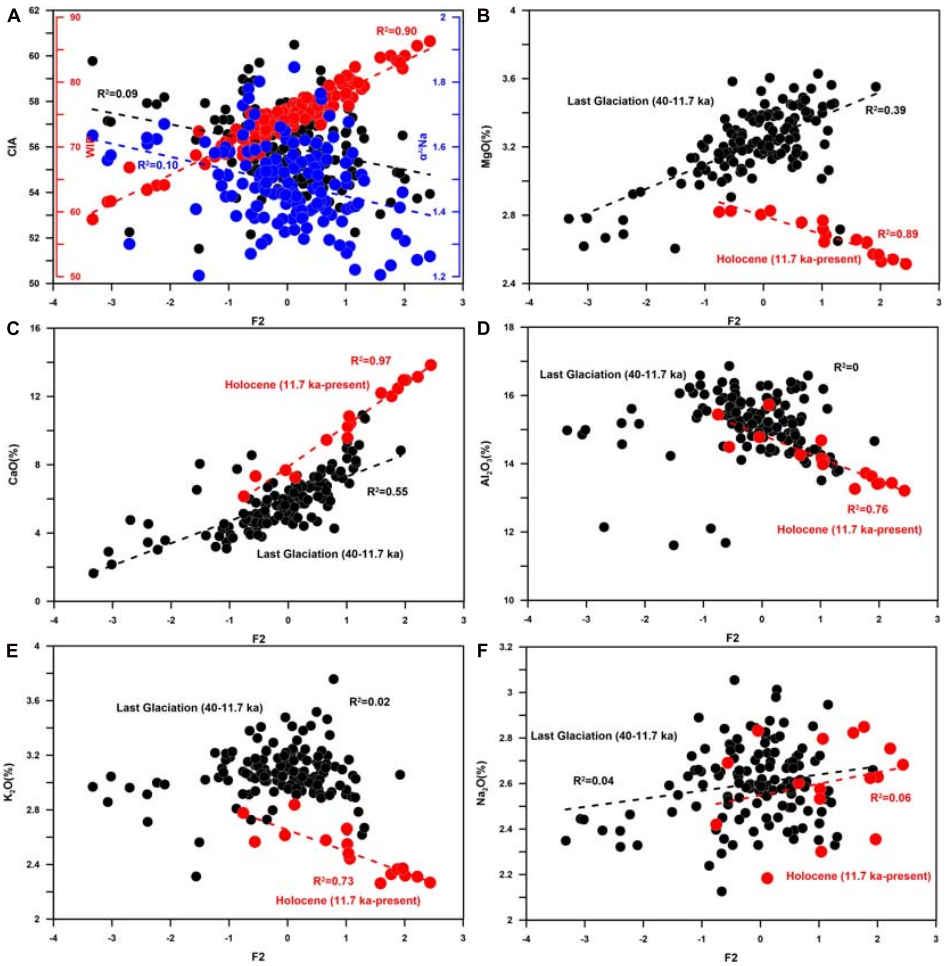

FIGURE 6 | Scatter diagrams between F2 and chemical weathering indexes and oxides. **(A)** Chemical weathering indexes (CIA-black circles, WIP-red circles and αAlNa-blue circles) vs F2 (the second factors extracted by principal component analysis); **(B)** MgO vs F2; **(C)** CaO vs F2; **(D)** Al_2O_3 vs F2; **(E)** K_2O vs F2; **(F)** Na_2O vs F2.

with F2 both in the last glaciation and the Holocene period. We thus suggest the F2 as control from carbonate input, both from the ocean and Ganges River (Garzanti et al., 2010). Dolomite and calcite could be the main carrier.

DISCUSSION

Chemical Weathering Intensity Responses to Monsoon Precipitation on Precessional Scale

Apart from climate, other driving forces including regional tectonic activity (Dixon et al., 2012; Liu et al., 2016a), rock types (Babechuk et al., 2014; Yang et al., 2004b; Liu et al., 2016b), vegetation (Galy et al., 2008; Shen et al., 2018), and geomorphology (Albert Galy, 1999; Yang et al., 2004a; Bouchez et al., 2012) also play important role in chemical weathering. The mountainous areas around the BoB have tectonically been stable during the last 40 ka. Weathering process has sensitive response to the distinctions in the lithology (e.g., ultramafic or granitic rocks) and landform (e.g., mountain or floodplain), mainly through climate change (precipitation/temperature). Long-term vegetation evolution is now suggested to be connected to the climate change (Galy et al., 2008; Shen et al., 2018). Thus, climate is suggested to be the main controlling factor of the chemical weathering intensity, since the last glacial period. Typical monsoon climate around the BoB provides us with abundant climate signatures, which could be carried by sediment particles and stored in the sink basins. Theoretically, our chronology framework has a resolution of 100–200 years and therefore has the ability to provide reliable climate signals above the millennium scale, excluding the negative processes such as signal attenuation and interference. Since the F1 shows co-variation with our indexes and faithfully record the chemical weathering dynamics and forcing mechanisms, we compared it with ISM precipitation, temperature, July solar radiation in 20°N, sea level and sedimentary rate to give a systematical analyses. The Indian monsoon intensity is affected by solar radiation, showing periodic changes on the precession scale, which is widely recorded in the Indian monsoon region (Prell and Kutzbach, 1987; Caley et al., 2011; Mohtadi et al., 2016). Our sedimentary records also show that chemical weathering indicators have roughly changed in two

precession cycles simultaneously with the July solar radiation in 20°N and monsoon precipitation over the last 40,000 years (**Figures 4A,C**, **7I**). Here, the Ti/Ca ratio is calculated to estimate the terrestrial input variation, based on the stable feature of Ti in hypergenesis and considerable part of biogenic input CaO (Hu et al., 2012; Chen et al., 2013; Clift et al., 2014; Cao et al., 2015; Li et al., 2017, 2019) and its efficiency has been confirmed by the roughly consistent trend of the sedimentary rate (Li et al., 2019). The results show that the Ti/Ca ratio change simultaneously with the chemical weathering indexes (**Figures 4**, **7D**). Indeed, along the studied core, enhancing the chemical weathering is associated with the increase in the terrestrial input, vice versa. This pattern is similar to the temperature and precipitation patterns in the Asian monsoon regions recorded by stalagmite $\delta^{18}O$ values (Wang et al., 2001; Yuan et al., 2004; Berkelhammer et al., 2012; Raza et al., 2017) and planktonic foraminifera *G. ruber* $\delta^{18}O$ values in the BoB (Kudrass et al., 2001; **Figures 7A,B,E,F**). Combined with the PCA results and the low sea level (**Figures 7C,H**) which could ensure that the deposition center is located in the Bengal Fan (Curray et al., 2003; Li et al., 2019), this indicates the ISM controlled the weathering/erosion processes on precessional scale. During the oxygen isotope stage III and the last deglaciation, higher temperature (Rashid et al., 2007; Raza et al., 2017), and monsoon precipitation (Prell and Kutzbach, 1987; Kudrass et al., 2001) improved the erosion and weathering intensity in the source area, causing overall higher records of CIA, α^{Al}Na, Ti/Ca values and lower records of WIP values in the BoB (**Figures 4**, **7D**). On the other hand, during the LGM when temperature and monsoon precipitation decreased to the lowest level (Prell and Kutzbach, 1987; Kudrass et al., 2001; Rashid et al., 2007; Raza et al., 2017), both physical erosion and chemical weathering in the source area significantly weakened. Additionally, ice cover in the high mountains expanded, causing decreased exposure area, and erosion production (Owen et al., 2002). Corresponding to this cold and dry climate conditions, sedimentary records in the BoB showed lower CIA, α^{Al}Na, and Ti/Ca values, as well as higher WIP values (**Figures 4**, **7D**). It was also supported by lower CIA* values (∼10 reduction) and decreased Himalayan material contribution (∼30% reduction) in an adjacent core SK187/PC33 (Tripathy et al., 2014). It is worth noting that chemical weathering and terrestrial inputs are not fully synchronized with changes in monsoon rainfall and solar radiation, especially during the second precessional cycle (20 ka to present; **Figure 7**). This is due to the fact that the short-cycle climate changes on the millennial scale break up such long-cycle changes on the orbital scale and special circumstances during the Holocene period, which will be discussed in depth later.

Chemical Weathering Intensity Responses to Temperature and Monsoon Precipitation on Millennial Scale

Corresponding to alteration of warm/cold period during the last deglaciation, the precipitation and temperature in the Indian monsoon regions show a simultaneously alteration of higher/lower values distribution (Kudrass et al., 2001; Rashid et al., 2007; Raza et al., 2017). The obvious simultaneously alteration of higher/lower values in the chemical weathering and terrestrial input proxies records (**Figures 4**, **7D**) provides us with evidences supporting our hypothesis that monsoon climate drives the chemical weathering on millennial scale. In detail, during the cold periods, e.g., H1 and YD, the lower CIA, α^{Al}Na, and Ti/Ca values and the higher WIP values (**Figures 4**, **7D**) indicate the weakened chemical weathering and erosion intensity. In the northeastern Indian Ocean, climate during these two events were characterized by obvious weakened ISM intensity with sharply decreased trends of precipitation and temperature (Kudrass et al., 2001; Rashid et al., 2007; Raza et al., 2017). The lower total organic carbon contents in the Arabian Sea can be considered as additional evidence for a weakened ISM conditions (Schulz et al., 1998). During this period, simultaneously decreased precipitation and temperature improved the ice expansion (Chauhan, 2003) and limited glacial melting process and the water-rock interactions, thus decreased weathering reaction rate. Opposite circumstance occurred during the warm periods, e.g., B/A and Early Holocene Climatic Optimum (EHCO), when the increased ISM intensity was recorded in the Asian monsoon regions, as evidenced by the higher volume of melted ice in the Himalaya mountains (Benn and Owen, 1998), warmer and wetter climate (Weber et al., 1997), the rainfall (Kudrass et al., 2001; Yuan et al., 2004; Fleitmann et al., 2007), and runoff reconstructions from the northeastern Indian Ocean, based on the planktonic foraminifera *G. sacculifer* shell Ba/Ca ratios (Gebregiorgis et al., 2016). The prevailing warm-wet climate conditions improved the weathering rate again, causing the higher CIA, α^{Al}Na, and Ti/Ca values, as well as the lower WIP values in our studied core (**Figures 4**, **7D**). Briefly, it supported our hypothesis that chemical weathering intensity responses to temperature and monsoon precipitation on millennial scale.

Contradiction Between Chemical Weathering and Indian Monsoon Records During the Holocene Period: Reason and Applicability

After a period of co-variation, the chemical weathering indicators, and the monsoon indicators showed opposite paths during the Holocene period: both monsoon rainfall and temperature reconstruction results showed that ISM was significantly stronger during the Holocene period, in comparison with the last glaciation (Kudrass et al., 2001; Rashid et al., 2007; Raza et al., 2017; **Figures 7A,E,F**), while the lower CIA, α^{Al}Na, and Ti/Ca values and the higher WIP values reflected weaker chemical weathering intensity and less terrestrial input (**Figures 4**, **7D**). Although, between 6 and 3 ka both stalagmites $\delta^{18}O$ from South Asia and SST reconstruction results in the northeastern Indian Ocean recorded a significant reduction in rainfall and temperature (Berkelhammer et al., 2012; **Figures 7B,F**), more factors were responsible for the low chemical weathering intensity values in the whole middle-late Holocene period on glacial-interglacial scale, especially that chemical weathering intensity started to be decreased after the EHCO, but the rainfall and temperature were still at a high level (**Figures 7A,C,E,F**). Indeed, the chemical weathering intensity,

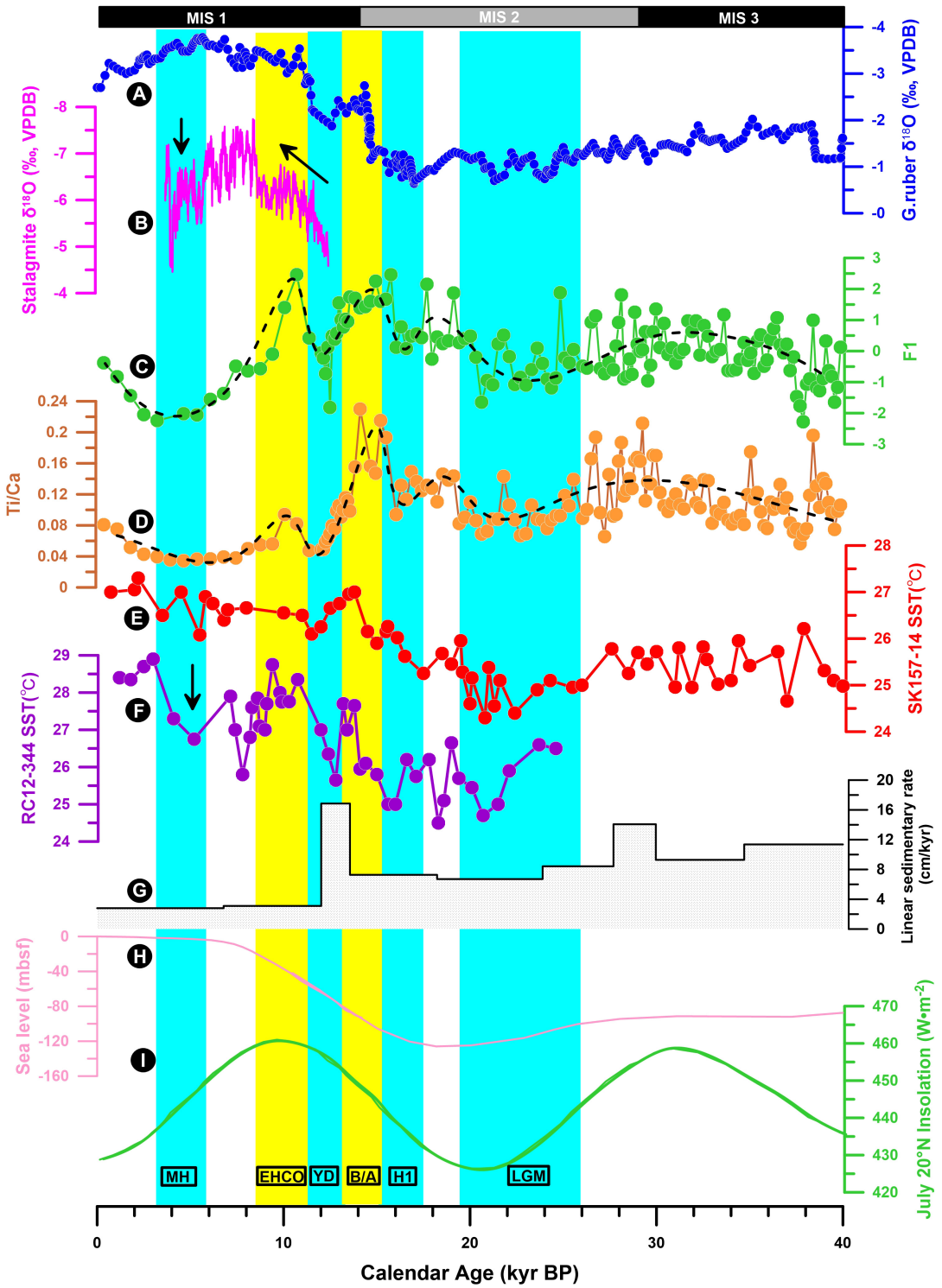

FIGURE 7 | Comparison of curves for chemical weathering intensity and climate proxies. **(A)** *G. ruber* $\delta^{18}O$ data from the core SO-126KL located in the northern BoB (Kudrass et al., 2001); **(B)** Mawmluh Cave stalagmite $\delta^{18}O$ data (Berkelhammer et al., 2012); **(C)** Chemical weathering stack of the core BoB-56; **(D)** Ti/Ca of the core BoB-56; **(E)** SST from the core SK157-14 from northeastern Indian Ocean (Raza et al., 2017); **(F)** SST from the core RC12-344 from northeastern Indian Ocean (Rashid et al., 2007); **(G)** Linear sedimentary rate of core BoB-56 (Li et al., 2019); **(H)** Sea level curve (Arz et al., 2007; Stanford et al., 2011); and **(I)** July insolation at 20°N (Prell and Kutzbach, 1987). The cyan and yellow color bars show the typical millennial scale intervals. LGM, Last Glacial Maximum; H1, Heinrich 1; B/A, Bølling/Allerød; YD, Younger Dryas; EHCO, Early Holocene Climatic Optimum; MH, Middle Holocene; and SST, Sea surface temperature. The dashed lines in **(C,D)** indicate the variation trends of the proxies.

revealed by clay minerals in the BoB, is consistent with that of the ISM intensity: e.g., a stronger intensity is identified in the Holocene, compared to the last glaciation (Li et al., 2018; Liu et al., 2019; Yu et al., 2020). In particular, clay mineral index smectite/(illite + chlorite) ratio and K/Al (molar ratio) in adjacent cores MD12-3417 and MD12-3418CQ also indicate increasing weathering since the Holocene period (Joussain et al., 2017). Moreover, it is widely accepted that the ISM during the Holocene was significantly stronger than the last glaciation (Kudrass et al., 2001; Rashid et al., 2007; Raza et al., 2017). A new question arises: why did the chemical weathering indicators (such as CIA, WIP, and α^{Al}Na) sensitivities reduced during the Holocene? Taking CIA as an example, the reasons may be, as follows:

The CIA is significantly affected by sediment grain size. The Ganges river "bank sediment-surface water suspension-bedload" depth profile CIA results show that the particles with a size of less than 0.1 μm in the bank sediment show the highest CIA value (CIA = 94). The particles with less than 2 μm in the bank sediment and surface water suspension show the similar CIA value (CIA = 82–85), while, the bulk sediments contain the lowest CIA value and the value of the surface suspension bulk CIA (CIA = 71) is higher than that of the bedload (CIA = 58; Garzanti et al., 2010, 2011; **Figure 8A**). Studies on the CIA value of bedload and suspension in G-B River show that the CIA value of suspension (mostly between 60 and 80) is significantly higher than that of bedload (mostly between 50 and 60; Singh and France-Lanord, 2002; Singh, 2009; Garzanti et al., 2010; **Figures 8B–D**). The bulk sediment CIA values of core BoB-56 are between 50 and 60 (**Figure 4A**), which is closer to the CIA of the bedload, with the clay fraction content of below 30% (**Figure 3**). Grain size of sediments in the core BoB-56 show a coarsening upward trend from the last glaciation to the Holocene period, with around 7% increase in the sand fractions (**Figure 3**). This seems to explain why fine particles (<2 μm), represented by clay minerals, indicates significantly stronger chemical weathering during the Holocene period than the last glaciation (Li et al., 2018; Yu et al., 2020), which is the opposite of the circumstance reflected by the bulk sediment geochemistry in this study (**Figure 4**).

The obvious difference of CIA between the two geomorphic units in the source region (high mountain terrain and low plain terrain) can be considered as another possible factor. The high mountain terrain is dominated by physical erosion and has relatively weak chemical weathering intensity, while, the low terrain, represented by the Indo-Gangetic Plain, has relatively

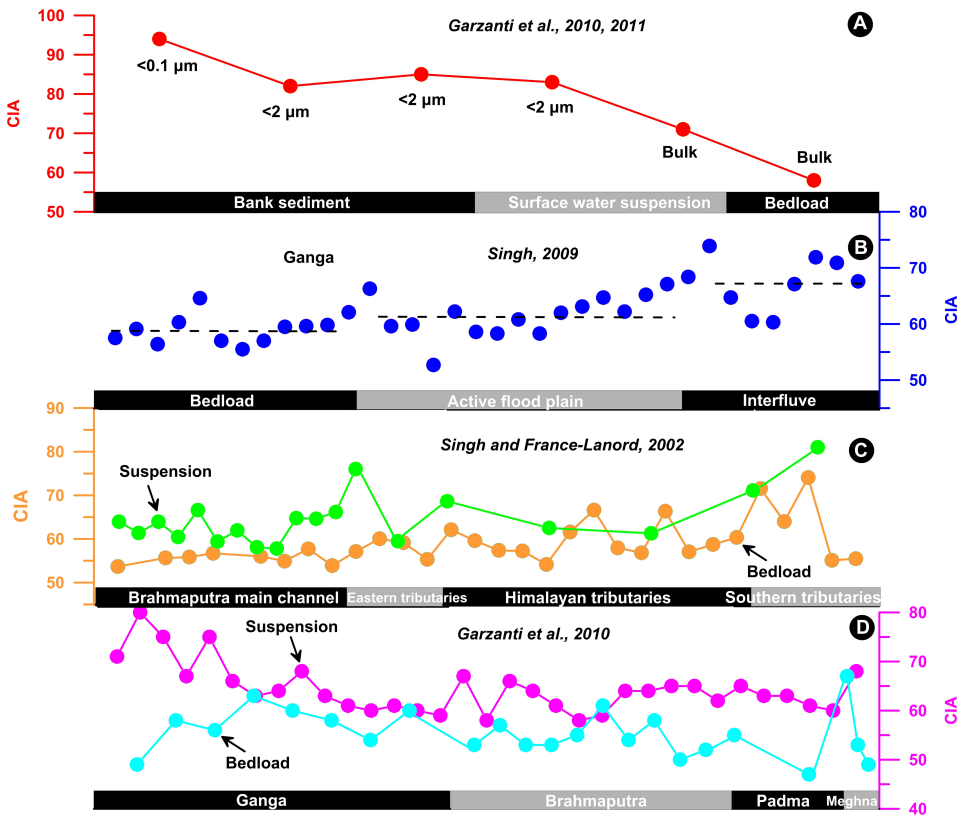

FIGURE 8 | CIA records in the source area (modified from published literature). **(A)** "Bank-suspension-bedload" CIA depth profile in the Ganga River (Garzanti et al., 2010, 2011); **(B)** CIA records in the Ganga River and its flood plain (Singh, 2009); **(C)** Bedload and suspension CIA records in the main channel and different tributaries of the Brahmaputra River (Singh and France-Lanord, 2002); and **(D)** Bedload and suspension CIA records in different rivers passing the Bangladesh (Garzanti et al., 2010).

stronger chemical weathering intensity and the CIA value is significantly higher than that of the mountain (Singh and France-Lanord, 2002; Owen, 2009; Singh, 2009). Under the background of significantly enhanced ISM during the Holocene, the erosion rate accelerated and the erosion yield and flux to the ocean increased significantly in both mountains and flood plains. As a result, the largest delta in the world, the G-B River delta, was constructed and improved. Subsequently, the continental shelf was submerged and the deposition center shifted from the Bengal Fan to the shelf, as a result of about 120–130 m sea level rise during the Holocene (Arz et al., 2007; Stanford et al., 2011), causing deduction in the sediment flux reaching the deep sea, hence, decrease in the Ti/Ca ratio during the Holocene (**Figure 7D**), though the ISM enhanced. Sediment in the floodplain are relatively fine and contribute a lot to the fine fractions, represented by clay minerals in the Bengal Fan. Smectite is originated mainly from the Indo-Gangetic Plain (Sarin et al., 1989; Huyghe et al., 2011). Therefore, the content of smectite in the BoB increased significantly under the background of intensified ISM during the Holocene, revealing strong chemical weathering dynamics (Joussain et al., 2016; Li et al., 2018; Yu et al., 2020). Studies of the adjacent cores MD12-3417 and MD12-3418CQ provide detail evidences of distinct weathering between high mountain terrain and the Indo-Gangetic Plain during the Holocene period (Joussain et al., 2017), which might be a supplement for our data during the Holocene period. Three stages, 9.2–7, 6.0–2.5, and 2.5 ka to present were divided and indicated more input from the mountains, the Indo-Gangetic Plain and plain soils due to anthropogenic activity, respectively. Due to the increase of physical erosion in the high mountain terrain, as the main sediment supplier, together with the grain size effect discussed above, the CIA value of bulk sediment decreased (**Figure 4A**). Therefore, it can be concluded that the bulk sediment geochemical-based weathering indicators, including CIA, WIP, and α^{Al}Na could not accurately reflect the chemical weathering dynamics of the source region and they appear to be a mixture of physical erosion and chemical weathering signals, which should be treated with caution.

CONCLUSION

1. Three geochemistry-based indexes, CIA, WIP, and α^{Al}Na, were extracted to estimate chemical weathering intensity dynamics. Overall, changes in the chemical weathering intensity were coincide with that of 20°N insolation, precipitation, and temperature changes, indicating that the ISM controlled weathering on precessional scales.
2. Obvious response between climate and chemical weathering occurred during the last deglaciation: stronger weathering during the B/A and EHCO periods, weaker weathering during the H1 and YD periods. The higher (lower) precipitation and temperature enhanced (weakened) the chemical weathering intensity during these warm (cold) periods, suggesting presence of control from the ISM on weathering on millennial scales.
3. Chemical weathering indexes showed significantly lower values during the Holocene period, which was inconsistence with the rising ISM precipitation and temperature. Besides the possible weakened monsoon during 6–3 ka, the grain size effect (finer particles are more sensitive than the bulk sediment especially when sand fractions increased), and relative geological location (sediment from the high mountain terrain has significant lower chemical weathering intensity than that from the low plain terrain) were suggested to be comprehensively responsible for this contradiction. Thus, the CIA, WIP, and α^{Al}Na values from bulk sediments cannot be representative of the chemical weathering intensity during the Holocene, as they seem to be a mixture of physical erosion and chemical weathering.

DATA AVAILABILITY STATEMENT

The original contributions presented in the study are included in the article/**Supplementary Material**, further inquiries can be directed to the corresponding author/s.

AUTHOR CONTRIBUTIONS

JL, XS, and SL proposed the topic, and conceived and designed the study. JL wrote the manuscript. HZ, PC, and XL carried out the experimental study and data analyses. H-JP, SK, and NK helped in data interpretation. SL collaborated with the corresponding author, XS, in the construction of the manuscript. All authors read and approved the final manuscript.

FUNDING

This work was supported by the National Program on Global Change and Air-Sea Interaction (GASI-GEOGE-06-03), the National Nature Science Foundation of China (41806081, U1606401, and 41676054), Natural Science Foundation of Shandong Province (ZR2019BD018), China-Thailand cooperation project "Research on Vulnerability of Coastal Zones," and the Taishan Scholar Program of Shandong.

ACKNOWLEDGMENTS

We would like to thank scientists from the First Institute of Oceanography, Ministry of Natural Resources, China, and the Phuket Marine Biological Center, Thailand, for sediment sampling.

SUPPLEMENTARY MATERIAL

The Supplementary Material for this article can be found online at: https://www.frontiersin.org/articles/10.3389/feart.2021.633713/full#supplementary-material

REFERENCES

Albert Galy, C. F.-L. (1999). Weathering processes in the Ganges–Brahmaputra basin and the riverine alkalinity budget. *Chem. Geol.* 159:30.

Arz, H. W., Lamy, F., Ganopolski, A., Nowaczyk, N., and Pätzold, J. (2007). Dominant Northern Hemisphere climate control over millennial-scale glacial sea-level variability. *Quat. Sci. Rev.* 26, 312–321. doi: 10.1016/j.quascirev.2006.07.016

Babechuk, M. G., Widdowson, M., and Kamber, B. S. (2014). Quantifying chemical weathering intensity and trace element release from two contrasting basalt profiles. Deccan Traps, India. *Chem. Geol.* 363, 56–75. doi: 10.1016/j.chemgeo.2013.10.027

Benn, D. I., and Owen, L. A. (1998). The role of the Indian summer monsoon and the mid-latitude westerlies inHimalayan glaciation-review and speculative discussion. *J. Geol. Soc.* 155, 353–363. doi: 10.1144/gsjgs.155.2.0353

Berkelhammer, M., Sinha, A., Stott, L., Cheng, H., Pausata, F. S. R., and Yoshimura, K. (2012). "An abrupt shift in the indian monsoon 4000 years ago," in *Geophysical Monograph Series: Climate Landscapes and Civilization*, eds L. Giosan, D. Q. Fuller, K. Nicoll, R. K. Flad, and P. D. Clift (Washington, D.C: AGU), 75–88. doi: 10.1029/2012gm001207

Berner, R. A. (1992). Weathering, plants, and the long-term carbon cycle. *Geochimica et Cosmochimica Acta* 56, 3225–3231. doi: 10.1016/0016-7037(92)90300-8

Bolton, C. T., Chang, L., Clemens, S. C., Kodama, K., Ikehara, M., Medina-Elizalde, M., et al. (2013). A 500,000 year record of Indian summer monsoon dynamics recorded by eastern equatorial Indian Ocean upper water-column structure. *Quat. Sci. Rev.* 77, 167–180. doi: 10.1016/j.quascirev.2013.07.031

Bouchez, J., Gaillardet, J., Lupker, M., Louvat, P., France-Lanord, C., Maurice, L., et al. (2012). Floodplains of large rivers: weathering reactors or simple silos? *Chem. Geol.* 33, 166–184. doi: 10.1016/j.chemgeo.2012.09.032

Caley, T., Malaizé, B., Zaragosi, S., Rossignol, L., Bourget, J., Eynaud, F., et al. (2011). New Arabian Sea records help decipher orbital timing of Indo-Asian monsoon. *Earth Planetary Sci. Lett.* 308, 433–444.

Cao, P., Shi, X., Li, W., Liu, S., Yao, Z., Hu, L., et al. (2015). Sedimentary responses to the Indian Summer Monsoon variations recorded in the southeastern Andaman Sea slope since 26ka. *J. Asian Earth Sci.* 114, 512–525. doi: 10.1016/j.jseaes.2015.06.028

Chauhan, O. S. (2003). Past 20,000-year history of Himalayan aridity: evidence from oxygen isotope records in the Bay of Bengal. *Curr. Sci.* 84, 90–93.

Chen, H.-F., Yeh, P.-Y., Song, S.-R., Hsu, S.-C., Yang, T.-N., Wang, Y., et al. (2013). The Ti/Al molar ratio as a new proxy for tracing sediment transportation processes and its application in aeolian events and sea level change in East Asia. *J. Asian Earth Sci.* 73, 31–38. doi: 10.1016/j.jseaes.2013.04.017

Clemens, S. C., and Prell, W. L. (2003). A 350,000 year summer-monsoon multi-proxy stack from the Owen Ridge. Northern Arabian Sea. *Mar. Geol.* 201, 35–51. doi: 10.1016/s0025-3227(03)00207-x

Clift, P. D., Wan, S., and Blusztajn, J. (2014). Reconstructing chemical weathering, physical erosion and monsoon intensity since 25Ma in the northern South China Sea: a review of competing proxies. *Earth-Science Rev.* 130, 86–102. doi: 10.1016/j.earscirev.2014.01.002

Curray, J., and Moore, D. (1971). Growth of the bengal deep-sea fan and denudation in the Himalayas. *Geol. Soc. Am. Bull.* 82, 563–572. doi: 10.1130/0016-7606(1971)82[563:gotbdf]2.0.co;2

Curray, J. R., Emmel, F. J., and Moore, D. G. (2003). The Bengal Fan: morphology, geometry, stratigraphy, history and processes. *Mar. Petroleum Geol.* 19, 1191–1223. doi: 10.1016/s0264-8172(03)00035-7

Dixon, J. L., Hartshorn, A. S., Heimsath, A. M., DiBiase, R. A., and Whipple, K. X. (2012). Chemical weathering response to tectonic forcing: a soils perspective from the San Gabriel Mountains. *California. Earth Planetary Sci. Lett.* 32, 40–49. doi: 10.1016/j.epsl.2012.01.010

Duplessy, J. C. (1982). Glacial to interglacial contrasts in the northern Indian Ocean. *Nature* 295, 494–498. doi: 10.1038/295494a0

Eiriksdottir, E. S., Gislason, S. R., and Oelkers, E. H. (2011). Does runoff or temperature control chemical weathering rates? *Appl. Geochem.* 26, S346–S349.

Fleitmann, D., Burns, S. J., Mangini, A., Mudelsee, M., Kramers, J., Villa, I., et al. (2007). Holocene ITCZ and Indian monsoon dynamics recorded in stalagmites from Oman and Yemen (Socotra). *Quat. Sci. Rev.* 26, 170–188. doi: 10.1016/j.quascirev.2006.04.012

Fleitmann, D., Burns, S. J., Mudelsee, M., Neff, U., Kramers, J., Mangini, A., et al. (2003). Holocene forcing of the Indian monsoon recorded in a stalagmite from Southern Oman. *Science* 300, 1737–1739. doi: 10.1126/science.1083130

Gaillardet, J., Dupré, B., and Allègre, C. J. (1999). Geochemistry of large river suspended sediments: silicate weathering or recycling tracer? *Geochimica et Cosmochimica Acta* 63, 4037–4051. doi: 10.1016/s0016-7037(99)00307-5

Galy, V., François, L., France-Lanord, C., Faure, P., Kudrass, H., Palhol, F., et al. (2008). C4 plants decline in the Himalayan basin since the Last Glacial Maximum. *Quat. Sci. Rev.* 27, 1396–1409. doi: 10.1016/j.quascirev.2008.04.005

Garzanti, E., Andó, S., France-Lanord, C., Censi, P., Vignola, P., Galy, V., et al. (2011). Mineralogical and chemical variability of fluvial sediments 2. Suspended-load silt (Ganga–Brahmaputra, Bangladesh). *Earth Planetary Sci. Lett.* 302, 107–120. doi: 10.1016/j.epsl.2010.11.043

Garzanti, E., Andò, S., France-Lanord, C., Vezzoli, G., Censi, P., Galy, V., et al. (2010). Mineralogical and chemical variability of fluvial sediments1. Bedload sand (Ganga–Brahmaputra, Bangladesh). *Earth Planetary Sci. Lett.* 299, 368–381. doi: 10.1016/j.epsl.2010.09.017

Garzanti, E., Limonta, M., Resentini, A., Bandopadhyay, P. C., Najman, Y., Andò, S., et al. (2013). Sediment recycling at convergent plate margins (Indo-Burman Ranges and Andaman–Nicobar Ridge). *Earth-Science Rev.* 123, 113–132. doi: 10.1016/j.earscirev.2013.04.008

Gebregiorgis, D., Hathorne, E. C., Sijinkumar, A. V., Nath, B. N., Nürnberg, D., and Frank, M. (2016). South Asian summer monsoon variability during the last 54 kyrs inferred from surface water salinity and river runoff proxies. *Quat. Sci. Rev.* 138, 6–15. doi: 10.1016/j.quascirev.2016.02.012

Gupta, A. K., Das, M., and Anderson, D. M. (2005). Solar influence on the Indian summer monsoon during the Holocene. *Geophys. Res. Lett.* 32, 1–4.

He, J., Garzanti, E., Dinis, P., Yang, S., and Wang, H. (2020). Provenance versus weathering control on sediment composition in tropical monsoonal climate (South China) - 1. Geochemistry and clay mineralogy. *Chem. Geol.* 558:119860. doi: 10.1016/j.chemgeo.2020.119860

Hu, D., Böning, P., Köhler, C. M., Hillier, S., Pressling, N., Wan, S., et al. (2012). Deep sea records of the continental weathering and erosion response to East Asian monsoon intensification since 14ka in the South China Sea. *Chem. Geol.* 32, 1–18. doi: 10.1016/j.chemgeo.2012.07.024

Huyghe, P., Guilbaud, R., Bernet, M., Galy, A., and Gajurel, A. P. (2011). Significance of the clay mineral distribution in fluvial sediments of the Neogene to Recent Himalayan Foreland Basin (west-central Nepal). *Basin Res.* 23, 332–345. doi: 10.1111/j.1365-2117.2010.00485.x

Jerolmack, D. J., and Paola, C. (2010). Shredding of environmental signals by sediment transport. *Geophys. Res. Lett.* 37, 1–5.

Joussain, R., Colin, C., Liu, Z., Meynadier, L., Fournier, L., Fauquembergue, K., et al. (2016). Climatic control of sediment transport from the Himalayas to the proximal NE Bengal Fan during the last glacial-interglacial cycle. *Quat. Sci. Rev.* 148, 1–16. doi: 10.1016/j.quascirev.2016.06.016

Joussain, R., Liu, Z., Colin, C., Duchamp-Alphonse, S., Yu, Z., Moréno, E., et al. (2017). Link between Indian monsoon rainfall and physical erosion in the Himalayan system during the Holocene. *Geochem. Geophys. Geosystems* 18, 3452–3469. doi: 10.1002/2016gc006762

Kudrass, H. R., Hofmann, A., Doose, H., Emeis, K., and Erlenkeuser, H. (2001). Modulation and amplification of climatic changes in the Northern Hemisphere by the Indian summer monsoon during the past 80 ky. *Geology* 29, 63–66. doi: 10.1130/0091-7613(2001)029<0063:maaocc>2.0.co;2

Li, J., Liu, S., Feng, X., Sun, X., and Shi, X. (2017). Major and trace element geochemistry of the mid-Bay of Bengal surface sediments: implications for provenance. *Acta Oceanol. Sinica* 36, 82–90. doi: 10.1007/s13131-017-1041-z

Li, J., Liu, S., Shi, X., Chen, M.-T., Zhang, H., Zhu, A., et al. (2020). Provenance of terrigenous sediments in the central Bay of Bengal and its relationship to climate changes since 25?ka. *Prog. Earth Planetary Sci.* 7:16.

Li, J., Liu, S., Shi, X., Zhang, H., Fang, X., Cao, P., et al. (2019). Sedimentary responses to the sea level and Indian summer monsoon changes in the central Bay of Bengal since 40?ka. *Mar. Geol.* 415:105947. doi: 10.1016/j.margeo.2019.05.006

Li, J., Liu, S., Shi, X., Zhang, H., Fang, X., Chen, M.-T., et al. (2018). Clay minerals and Sr-Nd isotopic composition of the Bay of Bengal sediments: implications for sediment provenance and climate control since 40 ka. *Quat. Int.* 493, 50–58. doi: 10.1016/j.quaint.2018.06.044

Liu, J., He, W., Cao, L., Zhu, Z., Xiang, R., Li, T., et al. (2019). Staged fine-grained sediment supply from the Himalayas to the Bengal Fan in response to climate change over the past 50,000 years. *Quat. Sci. Rev.* 212, 164–177. doi: 10.1016/j.quascirev.2019.04.008

Liu, J. T., Hsu, R. T., Hung, J.-J., Chang, Y.-P., Wang, Y.-H., Rendle-Bühring, R. H., et al. (2016a). From the highest to the deepest: the Gaoping River–Gaoping Submarine Canyon dispersal system. *Earth-Science Rev.* 153, 274–300. doi: 10.1016/j.earscirev.2015.10.012

Liu, Z., Zhao, Y., Colin, C., Stattegger, K., Wiesner, M. G., Huh, C.-A., et al. (2016b). Source-to-sink transport processes of fluvial sediments in the South China Sea. *Earth-Science Rev.* 153, 238–273. doi: 10.1016/j.earscirev.2015.08.005

Liu, S., Li, J., Zhang, H., Cao, P., Mi, B., Khokiattiwong, S., et al. (2020). Complex response of weathering intensity registered in the Andaman Sea sediments to the Indian Summer Monsoon over the last 40 kyr. *Mar. Geol.* 426:106206. doi: 10.1016/j.margeo.2020.106206

Liu, S., Shi, X., Liu, Y., Wu, Y., Yang, G., and Wang, X. (2013). Holocene paleoclimatic reconstruction based on mud deposits on the inner shelf of the East China Sea. *J. Asian Earth Sci.* 69, 113–120. doi: 10.1016/j.jseaes.2013.01.003

Mclennan, S. M., Hemming, S. R., Mcdaniel, D. K., and Hanson, G. N. (1993). Geochemical approaches to sedimentation, provenance, and tectonics. *Special Paper of the Geological Society of America* 284, 21–40. doi: 10.1130/SPE284-p21

Miriyala, P., Sukumaran, N. P., Nath, B. N., Ramamurty, P. B., Sijinkumar, A. V., Vijayagopal, B., et al. (2017). Increased chemical weathering during the deglacial to mid-Holocene summer monsoon intensification. *Sci. Rep.* 7:44310.

Mohtadi, M., Prange, M., and Steinke, S. (2016). Palaeoclimatic insights into forcing and response of monsoon rainfall. *Nature* 533, 191–199. doi: 10.1038/nature17450

Nesbitt, H. W., and Young, G. M. (1982). Early Proterozoic climates and plate motions inferred from major element chemistry of lutites. *Nature* 299, 715–717. doi: 10.1038/299715a0

Owen, L., Finkel, R., and Caffee, M. (2002). A note on the extent of glaciation throughout the Himalaya during the global Last Glacial Maximum. *Quat. Sci. Rev.* 21, 147–157. doi: 10.1016/s0277-3791(01)00104-4

Owen, L. A. (2009). Latest pleistocene and holocene glacier fluctuations in the Himalaya and tibet. *Quat. Sci. Rev.* 28, 2150–2164. doi: 10.1016/j.quascirev.2008.10.020

Parker, A. (1970). An index of weathering for silicate rocks. *Geol. Magazine* 107, 501–504. doi: 10.1017/s0016756800058581

Prell, W. L., and Kutzbach, J. E. (1987). Monsoon variability over the past 150,000 years. *J. Geophys. Res.* 92, 8411–8425. doi: 10.1029/jd092id07p08411

Rashid, H., Flower, B. P., Poore, R. Z., and Quinn, T. M. (2007). A 25ka Indian Ocean monsoon variability record from the Andaman Sea. *Quat. Sci. Rev.* 26, 2586–2597. doi: 10.1016/j.quascirev.2007.07.002

Raza, T., Ahmad, S. M., Steinke, S., Raza, W., Lone, M. A., Beja, S. K., et al. (2017). Glacial to Holocene changes in sea surface temperature and seawater δ18O in the northern Indian Ocean. *Palaeogeography Palaeoclimatol. Palaeoecol.* 485, 697–705. doi: 10.1016/j.palaeo.2017.07.026

Rodolfo, K. (1969). Sediments of the Andaman Basin, northeastern Indian Ocean. *Mar. Geol.* 7, 371–182. doi: 10.1016/0025-3227(69)90014-0

Romans, B. W., Castelltort, S., Covault, J. A., Fildani, A., and Walsh, J. P. (2016). Environmental signal propagation in sedimentary systems across timescales. *Earth-Science Rev.* 153, 7–29. doi: 10.1016/j.earscirev.2015.07.012

Sarin, M. M., Krishnaswami, S., Dilli, K., Somayajulu, B. L. K., and Moore, W. S. (1989). Major ion chemistry of the Ganga-Brahmaputra river system: weathering processes and fluxes to the Bay of Bengal. *Geochimica et Cosmochimica Acta* 53, 997–1009. doi: 10.1016/0016-7037(89)90205-6

Schulz, H., Rad, U. V., and Erlenkeuser, H. (1998). Correlation between Arabian Sea and Greenland climate oscillations of the past 110,000 years. *Nature* 393, 54–57. doi: 10.1038/31750

Sebastian, T., Nagender Nath, B., Venkateshwarlu, M., Miriyala, P., Prakash, A., Linsy, P., et al. (2019). Impact of the Indian Summer Monsoon variability on the source area weathering in the Indo-Burman ranges during the last 21?kyr: a sediment record from the Andaman Sea. *Palaeogeography Palaeoclimatol. Palaeoecol.* 516, 22–34. doi: 10.1016/j.palaeo.2018.11.035

Shen, X., Wan, S., Colin, C., Tada, R., Shi, X., Pei, W., et al. (2018). Increased seasonality and aridity drove the C4 plant expansion in Central Asia since the Miocene–Pliocene boundary. *Earth Planetary Sci. Lett.* 502, 74–83. doi: 10.1016/j.epsl.2018.08.056

Singh, M., Singh, I. B., and Müller, G. (2007). Sediment characteristics and transportation dynamics of the Ganga River. *Geomorphology* 86, 144–175. doi: 10.1016/j.geomorph.2006.08.011

Singh, P. (2009). Major, trace and REE geochemistry of the Ganga River sediments: influence of provenance and sedimentary processes. *Chem. Geol.* 266, 242–255. doi: 10.1016/j.chemgeo.2009.06.013

Singh, S. K., and France-Lanord, C. (2002). Tracing the distribution of erosion in the Brahmaputra watershed from isotopic compositions of stream sediments. *Earth Planetary Sci. Lett.* 202, 645–662. doi: 10.1016/s0012-821x(02)00822-1

Stanford, J. D., Hemingway, R., Rohling, E. J., Challenor, P. G., Medina-Elizalde, M., and Lester, A. J. (2011). Sea-level probability for the last deglaciation: a statistical analysis of far-field records. *Global Planetary Change* 79, 193–203. doi: 10.1016/j.gloplacha.2010.11.002

Taylor, S. R., and Mclennan, S. M. (1985). The continental crust: its composition and evolution. *J. Geol.* 94, 632–633.

Tripathy, G. R., Singh, S. K., and Ramaswamy, V. (2014). Major and trace element geochemistry of Bay of Bengal sediments: implications to provenances and their controlling factors. *Palaeogeography Palaeoclimatol. Palaeoecol.* 397, 20–30. doi: 10.1016/j.palaeo.2013.04.012

Walker, J. C. G., Hays, P. B., and Kasting, J. F. (1981). A negative feedback mechanism for the long-term stabilization of Earth's surface temperature. *J. Geophys. Res.: Oceans* 86, 9776–9782. doi: 10.1029/jc086ic10p09776

Wang, Y. J., Cheng, H., Edwards, R. L., An, Z. S., Wu, J. Y., Shen, C. C., et al. (2001). A high-resolution absolute-dated late Pleistocene Monsoon record from Hulu Cave. China. *Science* 294, 2345–2348. doi: 10.1126/science.1064618

Weber, M. E., Wiedicke, M. H., Kudrass, H. R., Hübscher, C., and Erlenkeuser, E. (1997). Active growth of the Bengal Fan during sea-level rise and highstand. *Geology* 25, 315–318. doi: 10.1130/0091-7613(1997)025<0315:agotbf>2.3.co;2

Xu, Z., Li, T., Clift, P. D., Wan, S., Qiu, X., and Lim, D. (2018). Bathyal records of enhanced silicate erosion and weathering on the exposed Luzon shelf during glacial lowstands and their significance for atmospheric CO 2 sink. *Chem. Geol.* 476, 302–315. doi: 10.1016/j.chemgeo.2017.11.027

Yang, S. Y., Jung, H. S., and Li, C. X. (2004a). Two unique weathering regimes in the Changjiang and Huanghe drainage basins: geochemical evidence from river sediments. *Sedimentary Geol.* 164, 19–34. doi: 10.1016/j.sedgeo.2003.08.001

Yang, S. Y., Li, C. X., Yang, D. Y., and Li, X. S. (2004b). Chemical weathering of the loess deposits in the lower Changjiang Valley, China, and paleoclimatic implications. *Quat. Int.* 117, 27–34. doi: 10.1016/s1040-6182(03)00113-7

Yu, Z., Colin, C., Bassinot, F., Wan, S., and Bayon, G. (2020). Climate-Driven weathering shifts between highlands and floodplains. *Geochem. Geophys. Geosystems* 21:e2020GC008936.

Yuan, D., Cheng, H., Edwards, R. L., Dykoski, C. A., Kelly, M. J., Zhang, M., et al. (2004). Timing, duration, and transitions of the last interglacial Asian monsoon. *Science* 304, 575–578. doi: 10.1126/science.1091220

Conflict of Interest: The authors declare that the research was conducted in the absence of any commercial or financial relationships that could be construed as a potential conflict of interest.